Discussion

The peak instantaneous impact pressures delivered by both of the tested oral water irrigators are much higher than the capillary, arterial, and venous pressures. Hence, these high pressures can directly damage the integrity of the blood capillary endothelium, resulting in hemorrhage, local transvascular fluid shift, interstitial flooding, and edema. These high jet impact pressures can also cause considerable lymphatic damage, especially at the microscopic level. This could result in tissue poisoning due to the accumulation of metabolic waste. Even the time-averaged pressures are quite high. The time-averaged impact pressures measured in the present investigation are quite consistent with our earlier theoretical predictions based on discharge flow measurements [12]. The current results further substantiate our hypothesis that the peak instantaneous pressures may be as high as five to nine times the time-averaged pressure for these devices [12].

The pressure intensities measured here are exerted by irrigators designed for home use. In dental practice, nozzle (needle) diameters as low as 0.016 cm I.D. (30 gage) are generally used. Since these irrigators have reciprocating positive displacement pumps, the discharge flow rate is independent of the tip diameter. However, the jet velocity increases with decreasing tip diameter. Obviously, the higher impact pressures generated by these devices present a greater destructive potential.

There is no evidence in the literature of any work performed to determine the jet pressure necessary to perform the cleaning action of water irrigators. If the claim of several authors that oral irrigators remove only loose oral debris is true, a small fraction of the measured instantaneous pressures should be sufficient to perform the cleaning action. Our theoretical calculations using particle dynamics suggest that pressure intensities of about 50–100 mmHg may be sufficient to remove loose oral debris. The use of pressures higher than necessary, apart from being wasteful, could be harmful to gingival tissue. Possibly, some chemical agents can be added to the water to help loosen the adhering debris and hence reduce required irrigation pressure.

Conclusions

The impact pressures delivered by the two widely used commercial oral water irrigators evaluated in the present work were found to be high enough to harbor potential for tissue damage. However, fundamental studies are needed to establish the damage thresholds for gingival epithelium and underlying tissue.

References

[1] S. S. Socransky, "Relationship of bacteria to the etiology of periodontal disease," *J. Dental Res.*, vol. 49, pp. 203–222, 1970.

[2] R. J. Genco, "Microbiology of periodontal disease," in *Periodontal Therapy*, 5th ed., H. M. Goldman and D. W. Cohen, Eds. St. Louis, MO: Mosby, 1973, pp. 178–195.

[3] R. C. Page and H. E. Schroeder, "Pathogenesis of inflammatory periodontal disease," *Lab. Invest.*, vol. 33, p. 235, 1976.

[4] J. J. Krajewski, J. Giblin, and A. W. Gargiulo, "Evaluation of a water pressure cleansing device as an adjunct to periodontal treatment," *Periodontics*, vol. 2, pp. 76–78, 1964.

[5] R. R. Lobene, "The effect of a pulsed water pressure device on oral health," *J. Periodontol.*, vol. 40, pp. 667–670, 1969.

[6] J. E. Phillips, "Effect of water irrigation on oral flora and gingival health," M.S. thesis, Marquette Univ., Milwaukee, WI, 1967.

[7] C. Sumner, "What is the value of water spray devices in maintaining adequate oral hygiene?" *Periodontal Abstr.*, vol. 14, p. 150, 1966.

[8] P. Crumley, "Letter to the editor," *Periodontal Abstr.*, vol. 15, p. 45, 1967.

[9] D. H. Fine and A. Baumhammers, "Effect of water pressure on stainable material on teeth," *J. Periodontol.*, vol. 41, p. 468, 1970.

[10] N. R. Covin, P. A. Lainson, J. H. Belding, and C. M. Fraleigh, "The effect of stimulating the gingiva by a pulsating water device," *J. Periodontol.*, vol. 44, pp. 286–293, 1973.

[11] A. A. Winter, "Rapid destruction caused by a water-irrigating device," *Periodontol Case Rep.*, vol. 3, pp. 11–14, 1981.

[12] N. P. Reddy, S. K. Kesavan, and B. R. Costarella, "Evaluation of oral water irrigation devices," *Eng. Med.*, vol. 14, no. 3, pp. 141–145, 1985.

[13] W. Seliger, "A technique for measuring the penetration of pulsating-jet oral irrigation," *Arch. Oral Biol.*, vol. 14, pp. 435–436, 1969.

An Efficient Algorithm for Spectral Analysis of Heart Rate Variability

RONALD D. BERGER, SOLANGE AKSELROD, DAVID GORDON, AND RICHARD J. COHEN

***Abstract*—We present a simple efficient algorithm for the derivation of a heart rate signal from the electrocardiogram. We demonstrate that the amplitude spectrum of this heart rate signal more closely matches that of the input signal to an integral pulse frequency modulation (IPFM) model of the heart's pacemaker than do the spectra of other ECG-derived heart rate signals. The applicability of this algorithm in cross-spectral analysis between heart rate and other physiologic signals is also discussed.**

I. Introduction

In a recent paper [1], DeBoer *et al.* compared two methods that employ spectral analysis for the study of heart rate variability. In a second paper [2], the same authors presented an evaluation of these two methods and of a third by testing each on a sequence of simulated *RR* intervals generated by an integral pulse frequency modulation (IPFM) model. An IPFM model is a device that integrates its input signal until the result of this integration reaches a preset threshold, at which point the device sends out a pulse, resets the integrator to zero, and begins the integration anew. Hyndman and Mohn [3] first suggested the IPFM model as a functional description of the sino-atrial node, and it remains a useful model for the mechanism by which the autonomic nervous system modulates heart rate. We can represent the operation of an IPFM model mathematically as

$$\bar{T} = \int_{t_k}^{t_{k+1}} (1 + m(t))\, dt. \tag{1}$$

$\bar{T}$ is the integrator's threshold value, which equals the duration of each *RR* interval were there no autonomic modulation of the SA node's intrinsic firing rate. The input signal is $s(t) = 1 + m(t)$, where all autonomic influences are lumped together in this model and are represented by $m(t)$. Obviously, when $m(t)$ increases, the *RR* interval shortens so that the instantaneous heart rate varies in proportion to $s(t)$. t_k is the time of the kth *R* wave.

In their evaluation of the performance of the various spectral techniques for analysis of heart rate variability, DeBoer *et al.* com-

Manuscript received September, 24, 1985; revised April 29, 1986.

R. D. Berger is with the Harvard–M.I.T. Division of Health Sciences and Technology and the Department of Electrical Engineering, Massachusetts Institute of Technology, Cambridge, MA 02139.

S. Akselrod is with the Department of Physics, Tel Aviv University, Tel Aviv, Israel.

D. Gordon is with the Department of Pediatric Cardiology, University of Illinois Medical Center, Chicago, IL 60612.

R. J. Cohen is with the Harvard–M.I.T. Division of Health Sciences and Technology and the Department of Physics, Massachusetts Institute of Technology, Cambridge, MA 02139.

IEEE Log Number 860911.

pared the results of each method to the spectrum of the input signal applied to the IPFM model that generated the simulated *RR* intervals. They considered the latter as the "true" heart rate spectrum. These investigators demonstrated that all three of the methods they considered introduce significant artifacts that corrupt the spectra, compared to the "true" spectrum.

For several years we have been studying heart rate variability [4]–[6]. DeBoer *et al.* [1] claimed we use one of the methods of analysis that they presented. We in fact employ an algorithm that differs from all three methods that DeBoer *et al.* [2] considered, and their careful analysis of these three methods has sparked our interest in similarly analyzing the performance of the heart rate spectral estimation technique we use. In this paper, we present our computationally efficient algorithm and demonstrate that the spectral estimate it yields almost exactly matches the "true" spectrum of the input signal to the IPFM model.

DeBoer *et al.* labeled the three types of power spectral estimates that they discussed as 1) the spectrum of intervals, 2) the spectrum of inverse intervals, and 3) the spectrum of counts. (For a detailed description of the methods involved in the computation of these spectra, see [1], [2].) The spectrum of intervals and the spectrum of inverse intervals are the discrete Fourier transforms (DFT) squared of sequences of numbers corresponding to the *RR* interval durations and their reciprocals, respectively. Each number in these sequences corresponds to a single beat; this obviously results in uneven sampling of the process in time. Since these numbers are evenly spaced only when plotted against beat number, the units of the frequency axis of these spectra are "cycles per beat" instead of "cycles per second." While the number of cycles per beat can be converted to an average number of cycles per second by multiplying the former by the average heart rate, it is not surprising that these spectra would differ in appearance from that of the input signal to an IPFM model that generated the *RR* intervals. For example, if the IPFM model's input were a sine wave, then there would be relatively fewer beats (and thus *RR* intervals) around the sine wave's minima, and relatively more when the sine wave is near its maxima. Thus, the spectrum of intervals and the spectrum of inverse intervals are the spectra not of a sampled sine wave, but rather of a distorted sinusoid-like signal that appears alternately stretched out and compressed. Clearly, such spectra will contain harmonics of the fundamental sine wave.

The spectrum of counts is the Fourier transform squared of a set of delta functions on a true time axis spaced according to the sequence of *RR* intervals. This power spectral estimate,[1] denoted $P_C(f)$, can be computed analytically as

$$P_C(f) = \frac{t_N}{N^2}\left[\left[\frac{N \sin(2\pi f t_N)}{2\pi f t_N} - \sum_{k=1}^{N} \cos(2\pi f t_k)\right]^2 + \left[\frac{N(\cos(2\pi f t_N) - 1)}{2\pi f t_N} + \sum_{k=1}^{N} \sin(2\pi f t_k)\right]^2\right] \quad (2)$$

where N is the number of delta functions in the record and t_k denotes the location in time of the kth impulse. (Note that (2) contains terms that compensate for the truncation effects that result from computing the Fourier transform of a finite set of delta functions.) Rompelman *et al.* [7] have presented a modification of this technique for efficient implementation on a personal computer. Since this spectrum is that of a true time signal, it is free of harmonic artifacts like those seen in the spectrum of intervals and the spectrum of inverse intervals. On the other hand, when the intervals are generated by an IPFM model, the spacing of the delta functions (not their amplitude) is modulated by the input signal applied to the model. Thus, artifacts will appear in the spectrum of counts at sidebands of the mean repetition rate, as in any frequency modulated process.

[1]In this paper, all power spectral estimates have been normalized by dividing by the square of the mean of the input signal.

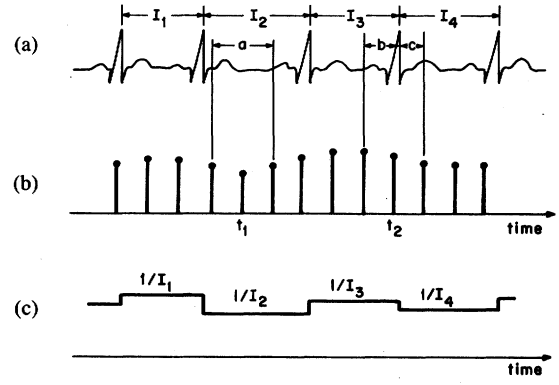

Fig. 1. (a) A segment of an ECG signal. (b) The heart rate samples corresponding to the ECG signal in (a), determined using our algorithm. The number of *RR* intervals within the local window centered at t_1 is a/I_2, and at t_2 is $b/I_3 + c/I_4$. The value of the heart rate at each sample point is taken to be the number of intervals that fell within the local window centered at that point divided by the width of the window, as described in the text. (c) The corresponding instantaneous heart rate signal. The value held during each interval is the reciprocal of the duration of that interval. The sample values in (b) are equivalent to those of the signal that would result from convolution of the signal in (c) with a rectangular window that is two sample intervals wide.

II. Description of Algorithm

In Fig. 1 we present a schematic description of the algorithm we use to derive a heart rate signal from the ECG signal. The steps involved are as follows. First, the ECG is sampled at a sufficiently high rate to determine the time locations of the *R* waves to whatever accuracy is desired. Next, a sampling rate for the heart rate signal is chosen. This is a true frequency (i.e., the heart rate samples will be evenly spaced in time at this frequency), and may be chosen arbitrarily, without regard to the mean heart rate or the frequency at which the ECG is sampled. A "local window" is then defined at each heat rate sample point as the time interval extending from the previous sample to the next. We then count the number of *RR* intervals (including fractions thereof) that occur within this local window. Examples of how we compute fractional *RR* intervals are shown in Fig. 1. The value r_i of the heart rate at each sample point is taken to be

$$r_i = f_r \cdot n_i/2 \quad (3)$$

where f_r is the sampling frequency of the resulting heart rate signal and n_i is the number of *RR* intervals that fell in the local window centered at the ith sample point. Finally, we estimate the heart rate power spectrum from the sequence of heart rate samples.[2]

Several observations may be made regarding this technique. Obviously, since the heart rate at each point depends on events in the ECG both in the recent past and the near future, this method cannot be employed in real-time analysis without incurring a delay. The heart rate signal produced by our algorithm may equivalently be viewed as samples of a stepwise continuous instantaneous heart rate signal convolved with a rectangular ("boxcar") window. This stepwise continuous instantaneous heart rate signal maintains an amplitude equal to the reciprocal of the current *RR* interval, for the duration of that *RR* interval [see Fig. 1(c)]. This signal differs from traditional tachometer signals (see for example Fig. 1(b) in [1]) in that the value held during the kth interval, (t_k, t_{k+1}), is $1/(t_{k+1} - t_k)$, not $1/(t_k - t_{k-1})$. As DeBoer *et al.* have recently noted [9], the traditional tachometer signal is flawed on two counts. First, the signal lags the ECG by an entire beat, which may be inconsequen-

[2]The spectrum can be computed from the sequence of heart rate samples using any of the standard spectral estimation methods [8]. We generally employ an FFT-based windowed periodogram method: in this paper for purposes of comparison to the results of DeBoer *et al.* [2], we have utilized the Bartlett window.

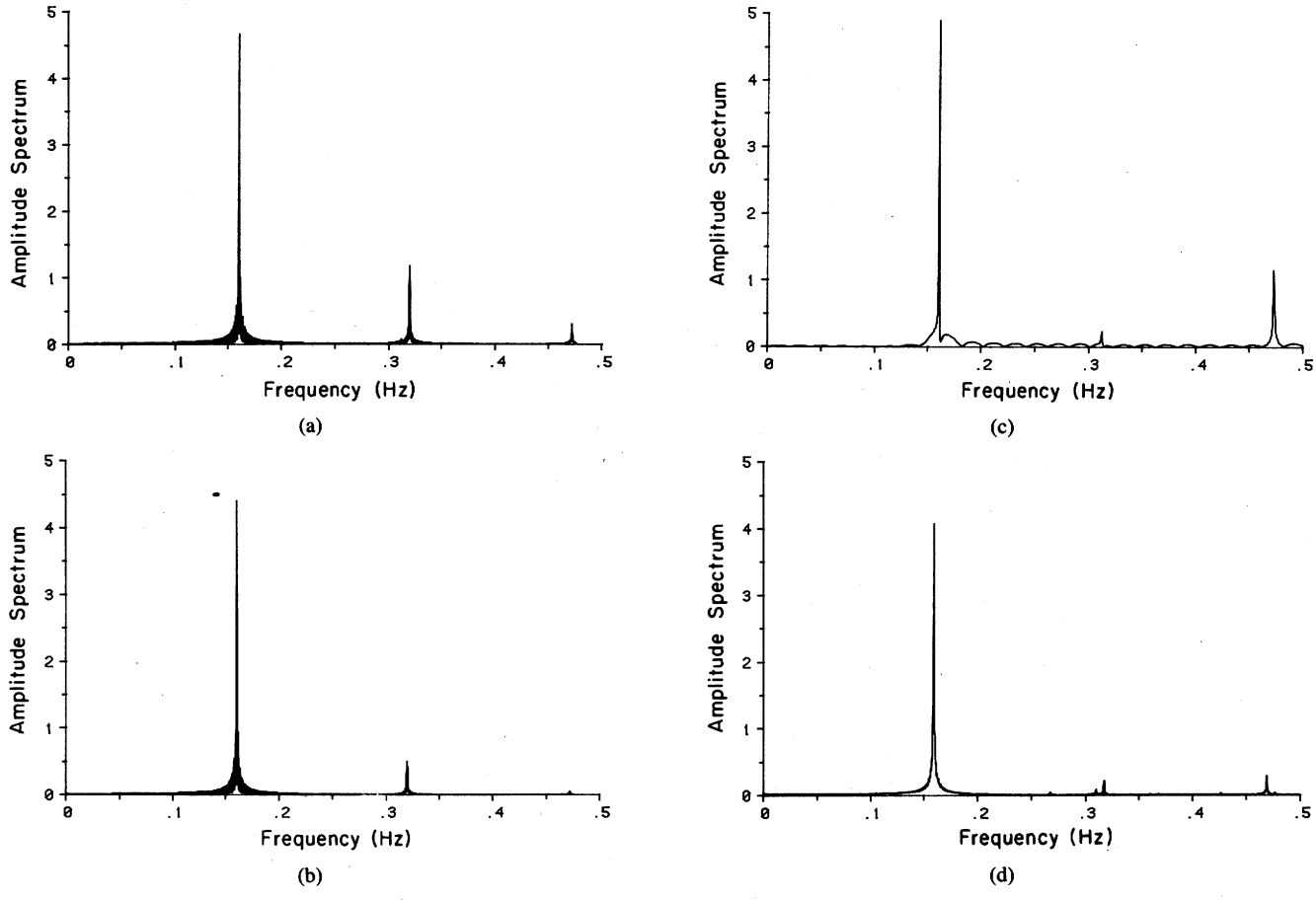

Fig. 2. Amplitude spectra from four different methods used to analyze the *RR* interval sequence resulting from an IPFM model, where the applied input signal was $s(t) = 1 + 0.3 \cos(2\pi f_m t)$. f_m was 0.16 Hz and the model's threshold $\bar{T}$ was 1.05 s. (a) Spectrum of intervals. (b) Spectrum of inverse intervals. (c) Spectrum of counts. (d) Spectrum of heart rate samples found using our algorithm. All four spectra were computed using 1024 *RR* intervals. The frequency axis in (a) and (b) was normalized to units of cycles per second by multiplication by the mean repetition rate, as described in the text. The spectrum of counts (c) was computed using (2). In (a), (b), and (d) the dc component was removed, and the amplitude spectra were then found by taking the square root of their corresponding power spectra, which were computed by taking the fast Fourier transform (FFT) squared of the time domain sequences. For the heart rate spectrum computed using our algorithm (d), the sampling rate f_r was 2.0 Hz, and before taking the square root of the corresponding power spectrum, it was first divided by the filter function $W(f)$ in (4).

tial in autospectral analysis, but can introduce artifactual phase shifts in cross spectra, for example, between heart rate and blood pressure or respiration. Second, the traditional tachometer signal provides a biased estimate of the heart rate since the lowest values are held for too short an amount of time, and the highest values are held for inappropriately long intervals. The mean heart rate thus appears higher than it should. The nondelayed instantaneous heart rate signal in Fig. 1(c) avoids both of these complications.

Convolution of the heart rate signal with the rectangular window has the effect on the power spectrum of multiplication by a low-pass filter. The shape of the filter $W(f)$ is

$$W(f) = \left[\frac{\sin(2\pi f/f_r)}{2\pi f/f_r}\right]^2 \tag{4}$$

where, again, f_r is the sampling frequency of the heart rate signal, so that $2/f_r$ is the width of the rectangular window in the time domain. This filter passes very little power beyond the Nyquist rate (i.e., $f_r/2$), and its effects can be compensated for in the band $0 < f < f_r/2$ by multiplying the power spectrum by $1/W(f)$. In practice, we apply a $1/W(f)$ correction, but consider the spectral estimate accurate only for $0 < f < f_r/4$, since the multiplication by $1/W(f)$ significantly amplifies any aliased power in the band $f_r/4 < f < f_r/2$.

While the choice for f_r is arbitrary, we typically choose $f_r = 4$ Hz, and similarly sample blood pressure and respiratory signals at 4 Hz. This is an appropriate sampling rate for the study of autonomic regulation, since it enables us to compute reliable spectral estimates between dc and 1 Hz, which represents the frequency band within which the autonomic nervous system has significant response. Furthermore, since the heart rate samples are spaced evenly in time and are synchronized with the samples of the other physiologic signals, cross-spectral estimates between these various signals are just as easy to compute as autospectra.

It should be noted that a power spectral estimate $P_S(f)$ for the stepwise continuous signal shown in Fig. 1(c) can be computed analytically without the need to generate samples of the signal using

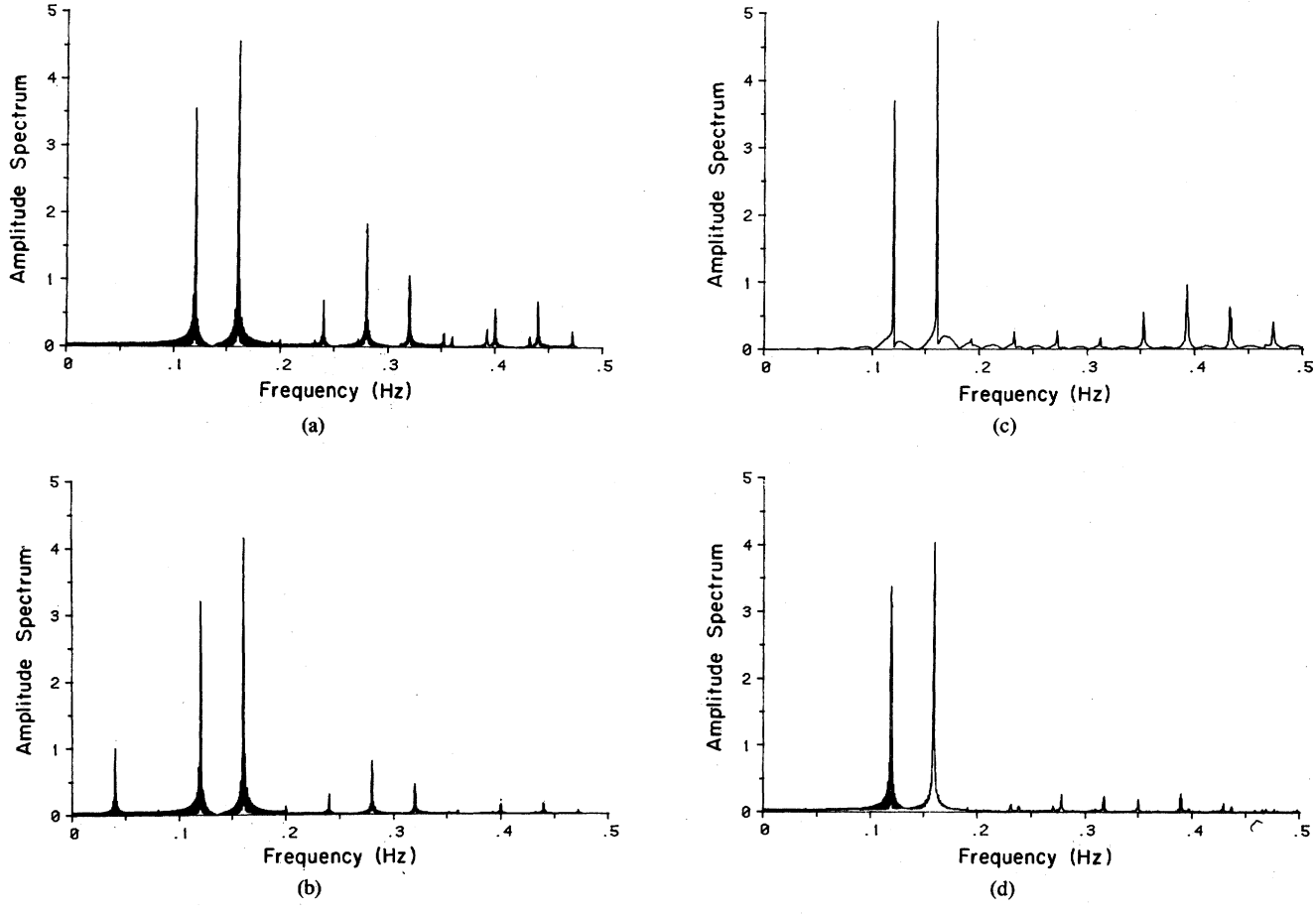

Fig. 3. Same as Fig. 2, but here the input signal applied to the IPFM model was $1 + 0.3 \cos(2\pi f_1 t) + 0.3 \cos(2\pi f_2 t)$, where $f_1 = 0.12$ Hz and $f_2 = 0.16$ Hz. The IPFM model threshold was again 1.05 s. The difference in heights of the two peaks at 0.12 and 0.16 Hz reflects different degrees of artifactual power leakage into side lobes of the respective peaks, despite the presence of equal amounts of power at these two frequencies in the input signal.

the relation

$$P_S(f) = \frac{t_N}{(2\pi f N)^2}\left[\left[\sum_{k=1}^{N}\left[\frac{1}{t_{k+1}-t_k} - \frac{N}{t_N}\right]\cdot(\cos(2\pi f t_{k+1}) - \cos(2\pi f t_k))\right]^2 + \left[\sum_{k=1}^{N}\left[\frac{1}{t_{k+1}-t_k} - \frac{N}{t_N}\right]\cdot(\sin(2\pi f t_{k+1}) - \sin(2\pi f t_k))\right]^2\right] \quad (5)$$

where N is the number of steps in the period of observation and t_k is the time at the beginning of the kth step. This technique generates spectral estimates whose only artifacts are the result of the small amount of generally high frequency power inevitably present in the discontinuities between adjacent steps. However, it is not a practical method because the evaluation of (5) for many different frequencies is computationally very burdensome and cannot be made more efficient through the use of FFT-like algorithms.

Furthermore, efforts to synthesize a discrete heart rate signal suitable for analysis with an FFT algorithm, by mere sampling without low-pass filtering of the instantaneous heart rate signal shown in Fig. 1(c), would cause the above-mentioned high frequency artifacts to become aliased into the physiologically important low frequency band of the power spectrum. It is important to note that while our method in effect generates heart rate sample values of a piecewise continuous signal that has undergone the necessary antialiasing filtering, the particular means by which we achieve the filtering operation is very efficient. Our method avoids the computational burden of actual digital convolution.

III. Comparison Between Our Method and Other Heart Rate Spectra

In order to demonstrate that the spectrum of the heart rate signal constructed using our algorithm is relatively free of artifacts, we performed the same simulations as DeBoer *et al.* did [2] by implementing an IPFM model on a digital computer. We then computed heart rate spectra first using the three methods they presented and then using ours. The spectra shown here are amplitude spectra (i.e., the square root of the power spectrum) as these accentuate the presence of harmonics and other artifacts.

Fig. 2 shows the results of the simulation where the IPFM model input signal was

$$s(t) = 1 + 0.3 \cos(2\pi f_m t) \quad (6)$$

and the modulation frequency f_m was 0.16 Hz and the IPFM threshold was 1.05 s.

All four spectra in Fig. 2 show a large peak at the modulation frequency (0.16 Hz). However, the spectrum of intervals [Fig. 2(a)] and the spectrum of inverse intervals [Fig. 2(b)] also contain a significant peak at the first harmonic (0.32 Hz) and a smaller one at the second harmonic (0.48 Hz) of the modulation frequency, that

are virtually absent in the heart rate spectrum computed with our algorithm [Fig. 2(d)]. Similarly, there is a sideband artifact at 0.472 Hz (0.952–0.48 Hz) in the spectrum of counts [Fig. 2(c)] that is totally absent in the spectrum computed with our algorithm.

Fig. 3 shows the results of a second simulation in which the input signal applied to the IPFM model was

$$s(t) = 1 + 0.3 \cos(2\pi f_1 t) + 0.3 \cos(2\pi f_2 t). \quad (7)$$

Here, again, the model's threshold was 1.05 s. The two modulation frequencies f_1 and f_2 were 0.12 and 0.16 Hz, respectively. These are the same parameters as those used by DeBoer *et al.* in their second simulation [2]. All of the spectra for this case show large peaks at the two modulation frequencies. In addition, the spectrum of intervals [Fig. 3(a)] and the spectrum of inverse intervals [Fig. 3(b)] possess artifacts at harmonics of both modulation frequencies, and the spectrum of counts [Fig. 3(c)] contains sideband artifacts at integer multiples of f_1 and f_2 away from the mean repitition rate of 0.952 Hz. Furthermore, the spectrum of inverse intervals [Fig. 3(b)] contains a component at 0.04 Hz, the difference between the two modulation frequencies. All of these artifacts are almost completely absent in the heart rate spectrum computed using our algorithm [Fig. 3(d)].

IV. Conclusion

The preponderance of influences that impinge on heart rate originate outside the heart, vary slowly compared to the heart rate, and are relatively insensitive to the actual timing of ventricular activations. For this reason, we feel that it seems more natural to characterize heart rate on a real-time axis, rather than against "beat number." The IPFM model is consistent with this description since it lumps autonomic control and all other factors that affect heart rate into a single time-varying signal. Our algorithm provides a computationally simple definition of a heart rate signal derived from the ECG, and as Figs. 2 and 3 demonstrate, the spectrum of this signal very closely matches that of the IPFM model input signal. In fact, because of the very way we define the heart rate signal, were this signal applied as the input to an IPFM device, the resulting sequence of *RR* intervals would be identical to the sequence of *RR* intervals from which the heart rate signal was derived.

References

[1] R. W. DeBoer, J. M. Karemaker, and J. Strackee, "Comparing spectra of a series of point events particularly for heart rate variability data," *IEEE Trans. Biomed. Eng.*, vol. BME-31, pp. 384–387, 1984.

[2] ——, "Spectrum of a series of point events, generated by the integral pulse frequency modulation model," *Med. Biol. Eng. Comput.*, vol. 23, pp. 138–142, 1985.

[3] B. W. Hyndman and R. K. Mohn, "A pulse modulator model for pacemaker activity," in *Dig. 10th Int. Conf. Med. Biol. Eng.*, 1973, p. 223.

[4] S. Akselrod, D. Gordon, F. A. Ubel, D. C. Shannon, A. C. Barger, and R. J. Cohen, "Power spectrum analysis of heart rate fluctuations: A quantitative probe of beat-to-beat cardiovascular control," *Science*, vol. 213, pp. 220–222, 1981.

[5] B. Pomeranz, R. J. B. MaCaulay, M. A. Caudill, I. Kutz, D. Adam, D. Gordon, K. M. Kilborn, A. C. Barger, D. C. Shannon, R. J. Cohen, and H. Benson, "Assessment of autonomic function in humans by heart rate spectral analysis," *Amer. J. Physiol.*, vol. 248, pp. H151–H153, 1985.

[6] S. Akselrod, D. Gordon, J. B. Madwed, N. C. Snidman, D. C. Shannon, and R. J. Cohen, "Hemodynamic regulation: Investigation by spectral analysis," *Amer. J. Physiol.*, vol. 249, pp. M867–M875, 1985.

[7] O. Rompelman, J. B. I. M. Snijders, and C. J. Van Spronsen, "The measurement of heart rate variability spectra with the help of a personal computer," *IEEE Trans. Biomed. Eng.*, vol. BME-29, pp. 503–510, 1982.

[8] S. M. Kay and S. L. Marple, "Spectrum analysis—A modern perspective," *Proc. IEEE*, vol. 69, pp. 1380–1419, 1981.

[9] R. W. DeBoer, J. M. Karemaker, and J. Strackee, "Description of heart-rate variability data in accordance with a physiological model for the genesis of heart beats," *Psychophysiology*, vol. 22, pp. 147–155, 1985.